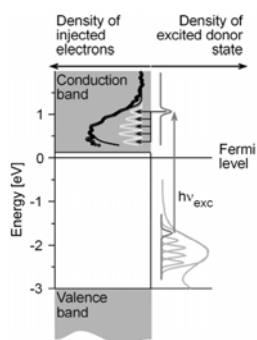


## CONTENTS

### Special issue on Theoretical Chemistry and Electrochemistry

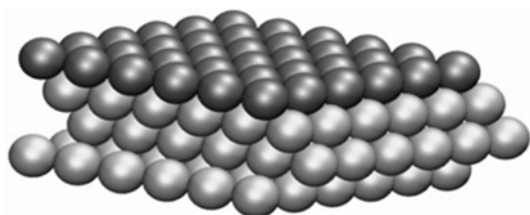
Foreword ..... 559



#### Test of theoretical models for ultrafast heterogeneous electron transfer with femtosecond two-photon photoemission data

Lars Gundlach, Tobias Letzig and Frank Willig ..... 561–574

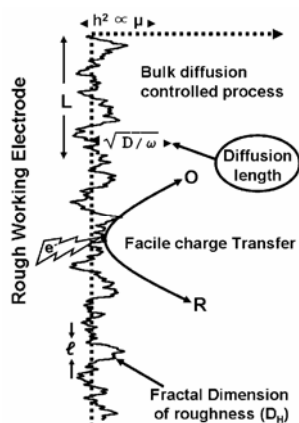
Illustration of the fully quantum mechanical model for ultrafast light-induced heterogeneous electron transfer where the vertical arrow illustrates the photon energy promoting the adsorbed molecule from the HOMO to the electronic excited state. Electronic states with different energies are occupied on the surface of the solid via electron transfer where the respective missing energy is used for excitation of a corresponding vibrational state in the ionized molecule.



#### Some properties of electrochemical nanostructures

E Santos, P Quaino, German Soldano and W Schmickler ..... 575–577

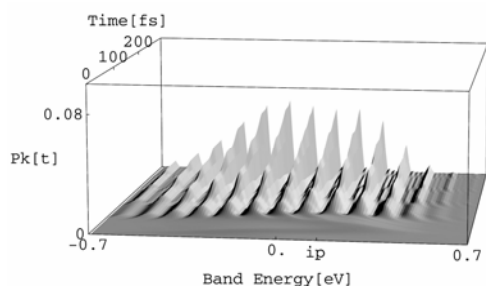
The density functional calculations indicate that Pt nanowires, clusters as well as monolayer of Pt on Au(111) are most suitable electrocatalysts for hydrogen evolution reaction.



#### Generalized Warburg impedance on realistic self-affine fractals: Comparative study of statistically corrugated and isotropic roughness

Rajesh Kumar and Rama Kant ..... 579–588

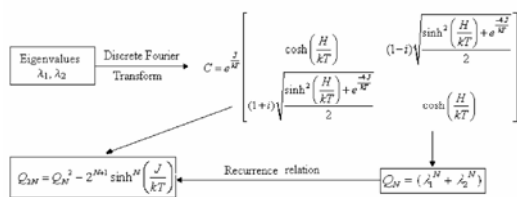
Electrode roughness strongly influences the diffusion or Warburg impedance. Roughness is modelled as a realistic self-affine fractal. Analysis of impedance response in Nyquist plot shows strong influence of three fractal morphological characteristics, viz. fractal dimension ( $D_H$ ), lower cutoff length ( $l$ ) and strength of fractality ( $\mu$ ). Our results explain anomalous behaviour of impedance for intermediate frequencies and their crossover to classical Warburg behaviour.



#### Theory of coherent molecule to surface electron injection: An analytical model

S Ramakrishna, T Seideman, F Willig and V May ..... 589–594

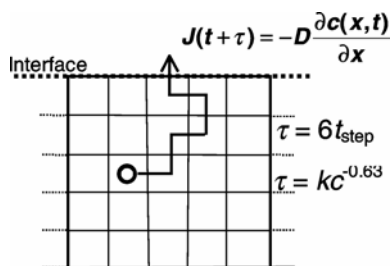
Coherent electron injection from a molecular electronic level to empty states of a substrate is explored using an electronic quasicontinuum model. The process is fundamental to several areas of interfacial science and its analysis leads to a simple and yet complete temporal description of the injection process.



**Partition function of nearest neighbour Ising models: Some new insights**

G Nandhini and M V Sangaranarayanan ..... 595–599

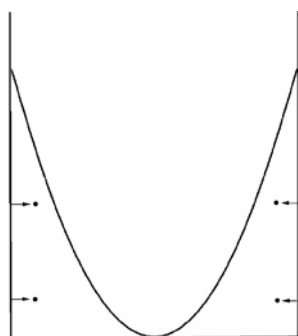
Employing the Discrete Fourier Transformation, a Hermitian Toeplitz matrix is constructed for one-dimensional Ising model, using the eigenvalues as the input. A new recurrence relation has been suggested for the partition function of Ising models.



**Simulation for memory effect of Fick's first law**

Koichi Aoki ..... 601–605

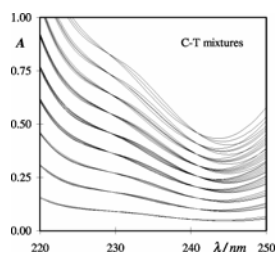
A new series of 1,3,4-thiadiazines carrying sydnone moiety are synthesized under solvent-free conditions by microwave irradiation.



**Graham's law of diffusion: Quantum analogy and non-ideality**

Chandrachur Das, Nabakumar Bera and Kamal Bhattacharyya ..... 607–615

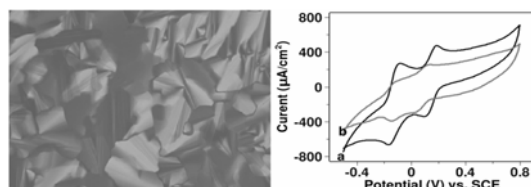
Modifications of Graham's law in presence of an attractive non-ideality are noted. A model confined quantum system is shown to simulate these results. Equivalent findings are revealed from statistical mechanics at the leading order. A statistical analog of the quantum virial theorem for confined systems is also obtained.



**Spectrometric mixture analysis: An unexpected wrinkle**

Robert de Levie ..... 617–627

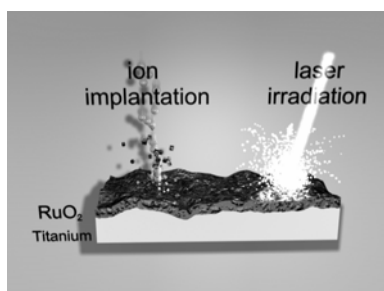
Inverse cancellation errors can cause data misinterpretation in trying to quantitate the individual components in a mixture when these components (here: caffeine and theobromine) have near-identical signatures.



**Electrochemical studies of redox probes in self-organized lyotropic liquid crystalline systems**

P Suresh Kumar and V Lakshminarayanan ..... 629–638

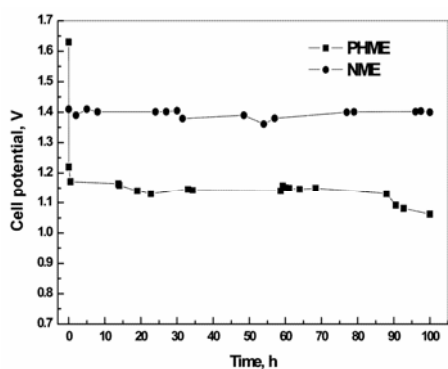
Electron transfer reactions have been studied in lyotropic liquid crystalline phase formed by a non-ionic surfactant Triton X-100 and water using electrochemical techniques. The ordered phase of liquid crystals, rich in water, mimic biological media and act as model systems for such studies. These studies reveal that the half peak potential shifts and changes in diffusion coefficient values compared to aqueous phase are dependent upon both the nature of the redox species and the medium.



**Surface modification of RuO<sub>2</sub> electrodes by laser irradiation and ion implantation: Evidence of electrocatalytic effects**

E Guerrini, A Colombo and S Trasatti ..... 639–646

Thermally prepared RuO<sub>2</sub> thin layers deposited on Ti supports were subjected in part to laser irradiation, in part to Kr bombardment. The voltammetric charge increased with surface treatment almost to the same extent for irradiation and bombardment. The electrocatalytic activity turned out much higher for Kr bombarded samples.



**Poly (vinyl alcohol) hydrogel membrane as electrolyte for direct borohydride fuel cells**

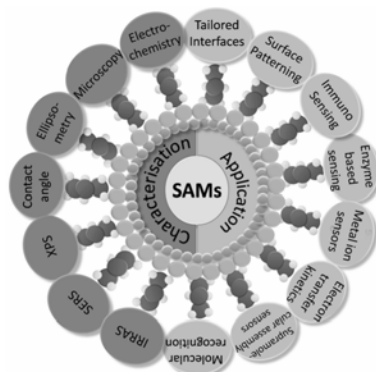
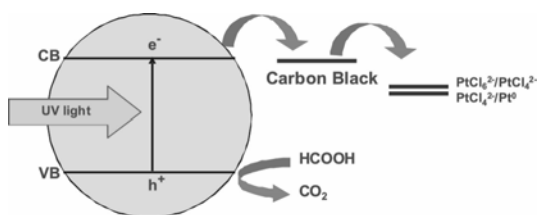
N A Choudhury, S K Prashant, S Pitchumani, P Sridhar and A K Shukla ..... 647–654

Poly (vinyl alcohol) hydrogel membrane electrolyte (PHME) is demonstrated as a cost-effective alternative to Nafion<sup>®</sup>-117 membrane electrolyte (NME) in Direct Borohydride Fuel Cell (DBFC), which gives a constant potential of ~1.2 V at a load current density of 10 mA cm<sup>-2</sup> for ~100 h at ambient temperature.

**Platinum-carbon black-titanium dioxide nanocomposite electrocatalysts for fuel cell applications**

Satheesh Sambandam, Vinodh Valluri, Wilaiwan Chanmanee, Norma R De Tacconi, Wesley A Wampler, Wen-Yuan Lin, Thomas F Carlson, Vijay Ramani and Krishnan Rajeshwar ..... 655–664

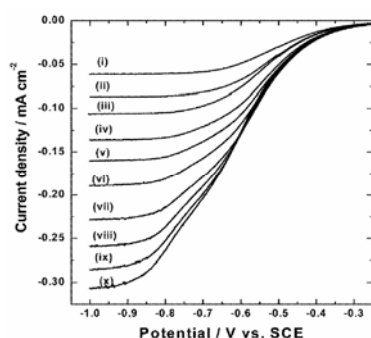
New generation Pt/C–TiO<sub>2</sub> nanocomposite electrocatalysts were prepared by a heterogeneous photocatalytic method. Galvanostatic data showed the superior stability of these materials against corrosion under anodic polarization relative to commercial benchmark fuel cell electrocatalysts. Electrochemical impedance spectroscopy provided information about the catalyst layer resistance.



**Tailoring self-assembled monolayers at the electrochemical interface**

S Varatharajan, Sheela Berchmans and V Yegnaraman ... 665–674

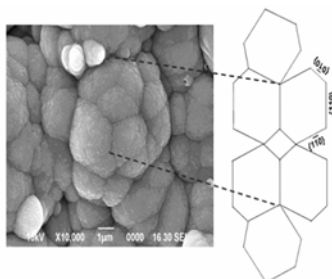
This review focuses on the formation, characterization and the tailoring of interfacial architecture of self-assembled monolayers (SAMs) with different receptors, catalytic materials, biomolecules, enzymes, antigen-antibody, etc for various applications.



### Electrochemical reduction of hydrogen peroxide on stainless steel

S Patra and N Munichandraiah ..... 675–683

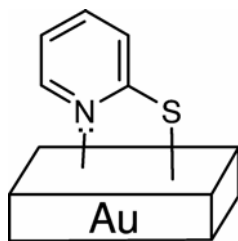
Electrochemical reduction of hydrogen peroxide is studied on a sand-blasted stainless steel electrode in an aqueous solution of  $\text{NaClO}_4$ . The cyclic voltammetric reduction of  $\text{H}_2\text{O}_2$  at low concentrations is characterized by a cathodic peak at  $-0.40$  V versus standard calomel electrode. From the rotating disc electrode study, diffusion co-efficient of  $\text{H}_2\text{O}_2$  and rate constant for reduction of  $\text{H}_2\text{O}_2$  are evaluated.



### Electrodeposition of $\text{BaCO}_3$ coatings on stainless steel substrates: Oriented growth in the presence of complexing agents

Sumy Joseph, Sarala Upadhyaya and P Vishnu Kamath ..... 685–691

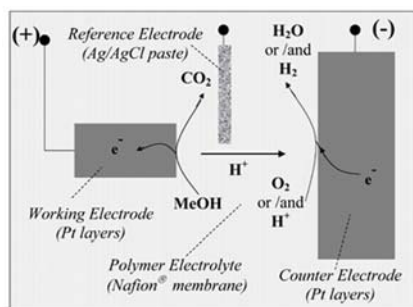
Observation of a pseudo three-fold symmetry generated by a trilling (three-fold twin) of electrodeposited  $\text{BaCO}_3$  crystallites has been presented.



### A comparative electrochemical study of electrosorbed 2- and 4-mercaptopyridines and their application as corrosion inhibitors at C60 steel

Nazly Hassan and Rudolf Holze ..... 693–701

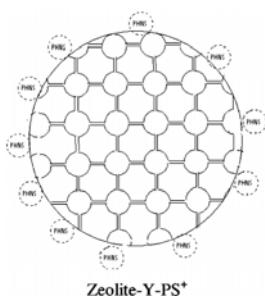
The electrosorption of 2- and 4-mercaptopyridine on gold and steel electrodes has been studied with several electrochemical techniques. Influences of the molecular structure on the adsorbate geometry derived from the obtained results are highlighted, they are also apparent in significant differences of corrosion inhibition efficiency.



### A Nafion®-based co-planar electrode amperometric sensor for methanol determination in the gas phase

K Wallgren and S Sotiropoulos ..... 703–709

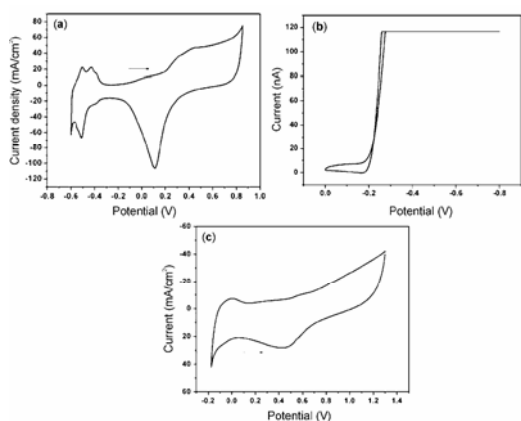
A co-planar all-solid electrode device, fabricated with all electrodes on the same face of a Nafion® polymer electrolyte membrane, is proposed for the direct amperometric detection of gaseous methanol both in nitrogen and air streams, with estimated detection limits of 1.2 and 1.4 Torr respectively.



### X-Ray photoelectron spectroscopic investigation of phenosafranine adsorbed onto micro and mesoporous materials

S Easwaramoorthi, K Ananthanarayanan, B Sreedhar and P Natarajan ..... 711–718

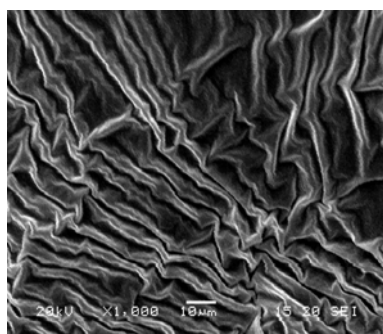
X-ray photoelectron spectra of phenosafranine adsorbed onto micro and mesoporous silicates show hydrogen bonded interaction between the dye and the silicate through the nitrogen atoms of the dye and silanol groups of the host materials.



**Imaging hydrogen oxidation activity of catalyst-coated per-fluoro sulfonic acid-polymer electrolyte membranes using Scanning Electrochemical Microscopy**

Meera Parthasarathy and Vijayamohan K Pillai ..... 719–725

A comparison of cyclic voltammograms of Pt/C in 0.5 M H<sub>2</sub>SO<sub>4</sub> (a), Pt disk ultra-microelectrode, (b) and Pt/C-Nafion film coated substrate electrode, (c) in 0.1 M LiClO<sub>4</sub> containing 10 mM HClO<sub>4</sub> at a scan rate of 25 mV/s along with imaging using scanning electrochemical microscopy enables a novel method to evaluate reactivity gradients of catalyst coated polymer electrolyte membranes, which is important to rectify problems related to catalyst distribution in H<sub>2</sub> oxidation activity as a function of potential applied to the Pt/C-Nafion film.



**Hydrogel membrane electrolyte for electrochemical capacitors**

S Sampath, N A Choudhury and A K Shukla ..... 727–734

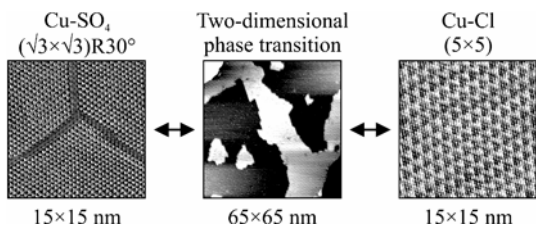
Doped poly(vinylalcohol)-based hydrogel electrolytes show very promising behaviour as electrolytes for supercapacitors with capacitances of the order of 100 F/g.



**Core-shell Au/Ag nanoparticles embedded in silicate sol-gel network for sensor application towards hydrogen peroxide**

Shanmugam Manivannan and Ramasamy Ramaraj ..... 735–743

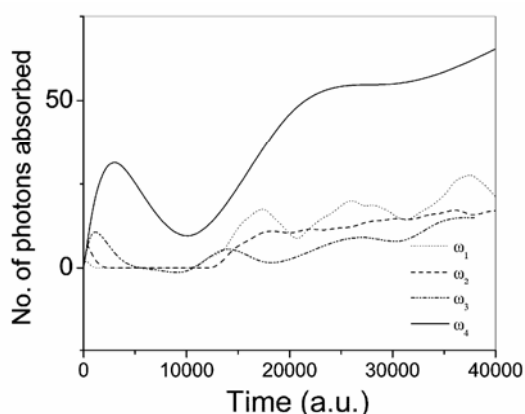
The electrocatalytic activity of core-shell Au<sub>100-x</sub>Ag<sub>x</sub> (molar ratio: x = 15, 27, 46 and 60) bimetallic nanoparticles embedded in methyl functionalized silicate sol-gel network modified electrode towards hydrogen peroxide and its amperometric sensing are investigated. The present study highlights the influence of molar composition of Ag nanoparticles in the Au-Ag core-shell bimetallic composition towards the electrocatalytic reduction and sensing of hydrogen peroxide in comparison to monometal Au and Ag nanoparticles.



**Structure transitions between copper-sulphate and copper-chloride UPD phases on Au(111)**

Ilya V Pobelov, Gábor Nagy and Thomas Wandlowski ..... 745–756

Using electrochemical scanning tunnelling microscopy we studied the formation and structure transitions of copper-sulphate and copper-chloride adlayers at the Au(111)/aqueous electrolyte interface.



**On optimal designing of low frequency polychromatic fields for facile photo-dissociation of model diatomic molecules**

S Ghosh, K Maji, R Sharma and S P Bhattacharyya ..... 757–766

The dissociation of a diatomic molecule in low frequency polychromatic fields of moderate intensities is studied. Genetic Algorithm is invoked to search out a set of four optimal non-resonant frequencies ( $\omega_1 - \omega_4$ ), intensities ( $\varepsilon_1 - \varepsilon_4$ ) and phase angles ( $\delta_1 - \delta_4$ ), for achieving a facile photo dissociation. Time-dependent Hellmann–Feynman theorem is used to gain insight into the frequency resolved energy absorption pattern. The ‘quantum phase space’ structures indicate occurrence of bond breaking dynamics akin to the classical one. The number of photon absorbed by a LiH molecule with time is shown.

The density operator for a two qubit system with correlated orientations (and polarizations  $P$ ), for example, is

$$\rho^{12} = \frac{1}{4} [(I^1 + P^1 \cdot \sigma^1)(I^2 + P^2 \cdot \sigma^2) + \sigma^1 \cdot \underline{\underline{C}} \cdot \sigma^2]$$

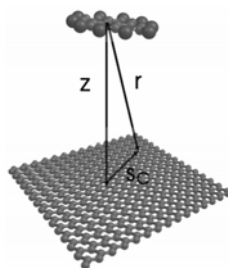
where  $\underline{\underline{C}}$  is the correlation tensor with coefficients ( $i, j = x, y, z$ )

$$C_{ij}^{12} = \langle \sigma_i^1 \sigma_j^2 \rangle - \langle \sigma_i^1 \rangle \langle \sigma_j^2 \rangle.$$

**Quantum entanglement and teleportation using statistical correlations**

Atul Kumar and Mangala Sunder Krishnan ..... 767–775

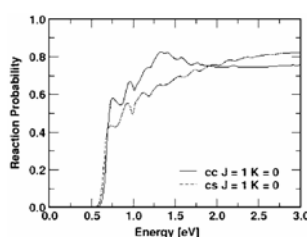
Correlation coefficients for two, three and four spin  $\frac{1}{2}$  particles (qubits) are used for quantifying entanglement and for describing quantum teleportation using density operators. We have introduced the correlated density matrix for two and many particles as an alternative to the impossibility of experimental preparation of an absolutely pure entangled state between particles and its subsequent redirection of members of the entangled state towards the sender and the receiver.



**Distance dependence of fluorescence resonance energy transfer**

R S Swathi and K L Sebastian ..... 777–787

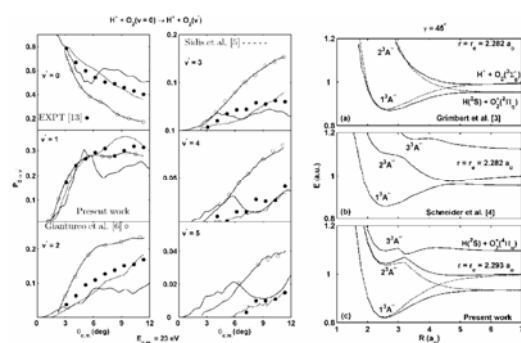
We study the process of resonance energy transfer from electronically excited fluorophores to various nano-systems. Our analysis of the process of energy transfer from a dye molecule to graphene leads to a  $(distance)^{-4}$  dependence of the rate, suggesting that it can be used as a nanoscopic ruler for measuring distances.



**Nonadiabatic quantum wave packet dynamics of the H + H<sub>2</sub> reaction including the coriolis coupling**

B Jayachander Rao and S Mahapatra ..... 789–795

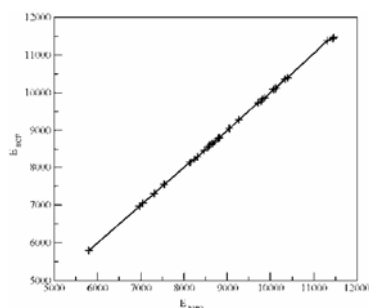
Coriolis coupling (CC) on the nonadiabatic H + H<sub>2</sub> ( $v = 0, j = 0$ ) → H<sub>2</sub> + H reaction dynamics are provided. CC effect on the reaction dynamics is investigated.



**Quantum dynamics of vibrational excitations and vibrational charge transfer processes in H<sup>+</sup> + O<sub>2</sub> collisions at collision energy 23 eV**

Saieswari Amaran and Sanjay Kumar ..... 797–803

Quantum mechanical results for the H<sup>+</sup> + O<sub>2</sub> system within the VCC–RIOS approximation employing the *ab initio* quasi-diabatic potential energy surfaces show overall agreement for the elastic/inelastic processes and some variance with the charge transfer processes in comparison with experiment. The likely ways to improve the results are discussed in terms of the inclusion of higher excited electronic states into the dynamics calculation.



**Effective harmonic oscillator description of anharmonic molecular vibrations**

Tapta Kanchan Roy and M Durga Prasad ..... 805–810

The validity of an effective harmonic oscillator approximation for anharmonic molecular vibrations is tested and compared with vibrational self-consistent field and vibrational configurational interaction results. The effective harmonic oscillator approximation provides a description of the anharmonic eigenstates very similar to the vibrational self-consistent field results.

$$L^TFL = \Lambda$$

is equivalent to

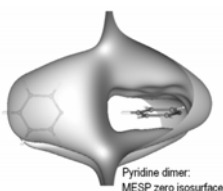
$$\begin{aligned} \sum_i c_i f_i &= \lambda_i \\ \sum_i c_i f_{ij} &= 0 \end{aligned}$$

Gaussian elimination gives the relations between  $f_i$ .

**A new scaling algorithm for predicting vibrational spectra of polyatomic molecules**

M Vijay Madhav and S Manogaran ..... 811–813

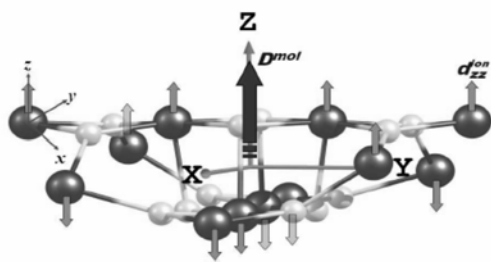
A relationship is proposed between the off-diagonal and diagonal force constants which is valid theoretically under harmonic approximation provided the  $L$  matrix is available from some theoretical calculation using  $L^TFL = \Lambda$ .



**Signatures of molecular recognition from the topography of electrostatic potential**

Dhimoy K Roy, P Balanarayan and Shridhar R Gadre ..... 815–821

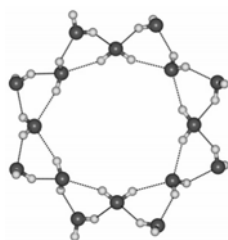
Topography of molecular electrostatic potential (MESP) is employed for defining recognition of two interacting molecular species.



**Computing magnetic anisotropy constants of single molecule magnets**

S Ramasesha, Shaon Sahoo, Rajamani Raghunathan and Diptiman Sen ..... 823–837

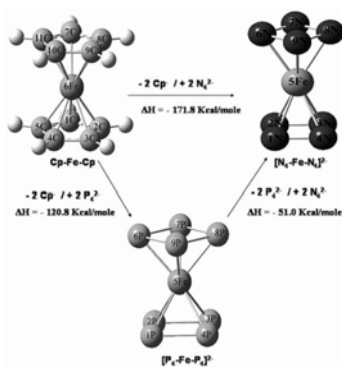
A theoretical approach to compute the molecular magnetic anisotropy parameters  $D_M$  and  $E_M$  for single molecule magnets in any given spin state of the Heisenberg exchange spin Hamiltonian are presented. A hybrid constant  $M_S$ -valence bond (VB) technique for solving spin conserving Hamiltonians that exploit full spatial and spin symmetries is also described.



**Structure and stability of spiro-cyclic water clusters**

M Elango, V Subramanian and N Sathyamurthy ..... 839–848

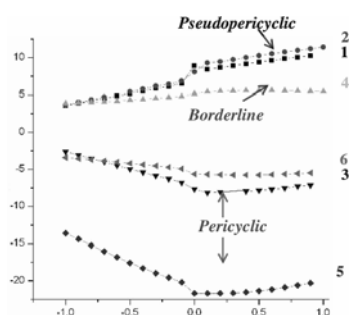
The structure and stability of spiro-cyclic water clusters containing up to 32 water molecules have been investigated. Although there exist energy minima lower than the spiro-cyclic clusters, they are stable in their own right.



### Bonding, aromaticity and reactivity patterns in some all-metal and non-metal clusters

S Duley, S Giri, A Chakraborty and P K Chattaraj ..... 849–858

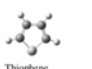


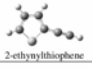

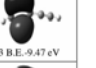
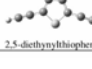


Several sandwich-like metal clusters have been studied at the B3LYP/6-311+G\* level of theory. Bonding and reactivity have been analysed through various geometrical parameters and conceptual density functional theory-based global reactivity descriptors. Aromaticity patterns have been understood in terms of the associated nucleus independent chemical shift values. Possibility of bond-stretch isomerism in some doped clusters is explored. Preferable sites for electrophilic and nucleophilic attacks have been identified using different local reactivity descriptors.



### Fluorine effect on pericyclic and pseudopericyclic processes: Evidences and *ab initio* theory

Lakshminarayanan Akilandeswari, Madhavan Jacob and Ponnambalam Venuvanalingam ..... 859–866

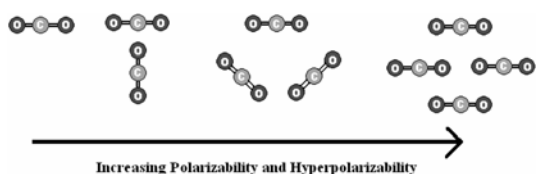
Fluorine substitution increases the pseudopericyclic character of the electrocyclic ring opening reactions of 2-pyranol and pyran through its lone pair participation in the cyclic overlap of orbitals while it does not affect the pseudopericyclic nature of the electrocyclic ring opening reaction of 2-pyrone.

Molecule	Dyson HOMO	Dyson HOMO-1
 Thiophene	 P3 B.E.-9.06 eV	 P3 B.E.-9.31 eV
 2-ethynylthiophene	 P3 B.E.-8.71 eV	 P3 B.E.-9.47 eV
 2,5-diethynylthiophene	 P3 B.E.-8.52 eV	 P3 B.E.-9.60 eV

### Electronic structure analysis and vertical ionization energies of thiophene and ethynylthiophenes

Raman K Singh and Manoj K Mishra ..... 867–872

Dyson orbitals and the corresponding vertical ionization energies for thiophene and ethynylthiophenes have been computed using different decouplings of electron propagator theory. Ring  $\pi$  and ethynyl  $\pi_{c-c}$  electron density distribution of these Dyson orbitals have been analysed for NLO/electrochemical response.



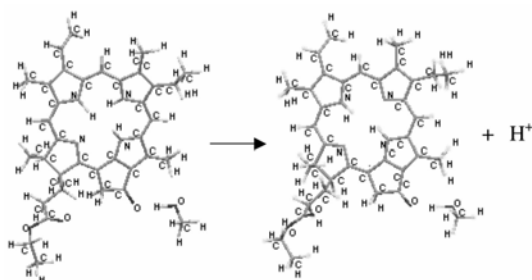
### Electronic absorption spectra and nonlinear optical properties of CO<sub>2</sub> molecular aggregates: A quantum chemical study

Tarun K Mandal, Sudipta Dutta and Swapan K Pati ..... 873–880

The quantum chemical calculations of non-linear optical properties of the CO<sub>2</sub> aggregates suggest the application of dense CO<sub>2</sub> in opto-electronic devices.

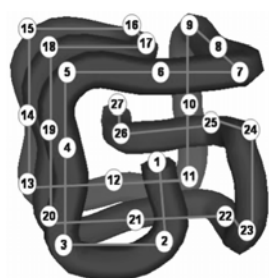
### Comparison between implicit and hybrid solvation methods for the determination of $pK_a$ of mono-protonated form of 13<sup>2</sup>-(demethoxycarbonyl) pheophytin *a* in methanol

Nital Mehta and Sambhu N Datta ..... 881–886



Implicit solvation method (dielectric polarisable continuum model, DPCM) and hybrid solvation method (cluster–continuum model) are adopted to calculate the  $pK_a$  of mono-protonated form of 13<sup>2</sup>-(demethoxycarbonyl) pheophytin *a* (Pheo) in methanol. The  $pK_a$  values of PheoH<sup>+</sup> calculated by DFT–DPCM and cluster–continuum methods are 6.12 and 4.70 respectively while the observed value is 4.14. The good performance of the cluster–continuum model over pure continuum model can be attributed to the hydrogen bonding interaction between the solute and the solvent.

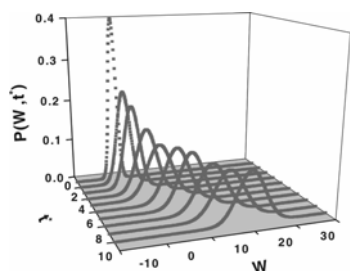




**Statistical theory of neutral protein evolution by random site mutations**

Arnab Bhattacharjee and Parbati Biswas ..... 887–896

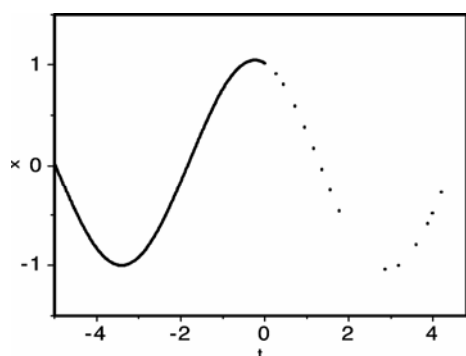
A self-consistent mean-field theory is developed to evaluate protein neutrality through random single and multiple point mutations by mapping real proteins into a cubic lattice. The results obtained from the theory are in good agreement with the exact enumeration results of the lattice protein and selected real proteins.



**Work distribution for a particle moving in an optical trap and non-Markovian bath**

Alok Samanta, K Srinivasu and Swapan K Ghosh ..... 897–904

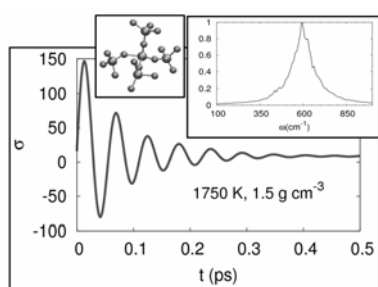
An exact analytical expression of work distribution has been obtained for a system consisting of a colloidal particle trapped in an optical harmonic potential, which is pulled at a constant velocity through a solution represented by a non-Markovian bath composed of an infinite set of harmonic oscillators.



**Growth and decay of large fluctuations far from equilibrium**

Shrabani Sen, Syed Shahed Riaz and Deb Shankar Ray ... 905–911

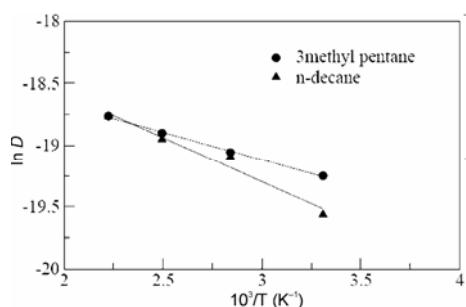
The principle of detailed balance takes care of, on an average, a balance of input of energy into the system through thermal fluctuation and output of energy from the system due to dissipation in a thermally equilibrated system. A ‘detailed balance’ like condition in the steady state is manifested in the time reversal symmetry between growth and decay of fluctuations far from equilibrium in a non-linear dissipative system characterized by a limit cycle attractor.



**Evaluation of collective transport properties of ionic melts from molecular dynamics simulations**

Manish Agarwal and Charusita Chakravarty ..... 913–919

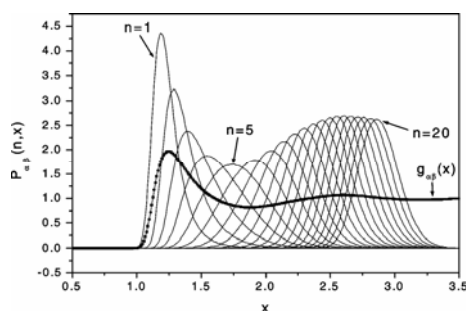
Molecular dynamics simulations of beryllium fluoride have been carried out using a rigid-ion potential model. Transport measures such as the viscosities and ionic conductivities are computed using the Green–Kubo formulation. In addition, structural relaxation times and high-frequency IR-active modes are computed from the pressure and charge-flux auto correlation functions respectively.



**A comparative molecular dynamics study of diffusion of n-decane and 3-methyl pentane in Y zeolite**

F G Pazzona, B J Borah, P Demontis, G B Suffritti and S Yashonath ..... 921–927

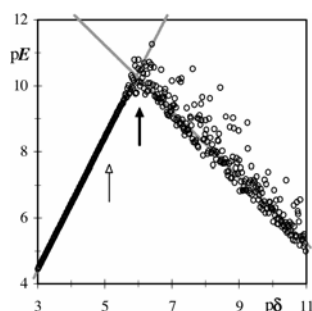
Hydrocarbons in zeolite Y exhibits an anomalous behaviour whereby 3-methyl pentane with larger cross section exhibits a higher diffusivity at low temperatures. This has its origin in the Levitation effect. Lower activation energy for 3-methyl pentane (3.7 kJ/mol) as compared to n-decane (6.0 kJ/mol) confirming the origin lies in the Levitation effect.



### ***n*th-Nearest neighbour distribution functions of a binary fluid mixture**

P Sur and B Bhattacharjee ..... 929–934

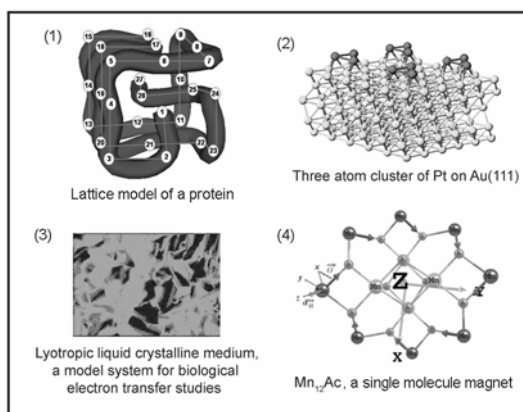
A general hierarchical approach for obtaining the *n*th nearest neighbour distribution (NND) functions (for  $n = 1, 2, 3, \dots$ ) of the binary mixtures from the partial pair correlation functions is presented. Results are compared with MD simulation for L–J binary mixtures showing reasonable matching for smaller *n* values particularly at higher density. The average *n*th nearest neighbour distance shows interesting feature.



### **An improved numerical approximation for the first derivative**

Robert de Levie ..... 935–950

Analysis of the precise nature of cancellation noise yields an improved algorithm for numerical differentiation by central differencing.



*Cover picture:* (1) Lattice model of a protein; for details see the paper by A Bhattacharjee and P Biswas (pp 887–896). (2) Three atom cluster of Pt on Au(111); for details see the paper by E Santos *et al* (pp 575–577). (3) Lyotropic liquid crystalline medium, a model system for biological electron transfer studies; for details see the paper by P Suresh Kumar and V Lakshminarayanan (pp 629–638). (4)  $Mn_{12}Ac$ , a single molecule magnet; for details see the paper by S Ramasesha *et al* (pp 823–837).